A melanocyte lineage program confers resistance to MAP kinase pathway inhibition

Citation	Johannessen, C. M., L. A. Johnson, F. Piccioni, A. Townes, D. T. Frederick, M. K. Donahue, R. Narayan, et al. 2014. "A melanocyte lineage program confers resistance to MAP kinase pathway inhibition." Nature 504 (7478): 138-142. doi:10.1038/nature12688. http://dx.doi.org/10.1038/nature12688.
Published Version	doi:10.1038/nature12688
Accessed	February 16, 2015 4:08:25 PM EST
Citable Link	http://nrs.harvard.edu/urn-3:HUL.InstRepos:12717516
Terms of Use	This article was downloaded from Harvard University's DASH repository, and is made available under the terms and conditions applicable to Other Posted Material, as set forth at http://nrs.harvard.edu/urn-3:HUL.InstRepos:dash.current.terms-of-use#LAA

(Article begins on next page)

A melanocyte lineage program confers resistance to MAP kinase pathway inhibition

Cory M. Johannessen[1,2,3], **Laura A. Johnson**[1,2,5], **Federica Piccioni**[1], **Aisha Townes**[1], **Dennie T. Frederick**[4], **Melanie K. Donahue**[1], **Rajiv Narayan**[1], **Keith T. Flaherty**[4], **Jennifer A. Wargo**[4], **David E. Root**[1], and **Levi A. Garraway**[1,2,3]

[1]The Broad Institute of Harvard University and Massachusetts Institute of Technology, Cambridge, MA 02142, USA

[2]Department of Medical Oncology, Dana-Farber Cancer Institute, Boston, MA 02115, USA

[3]Harvard Medical School, Boston, MA 02115, USA

[4]Department of Surgical Oncology, Medical Oncology and Dermatology, Massachusetts General Hospital, Boston, MA, 02114, USA

Abstract

BRAF^{V600E}-mutant malignant melanomas depend on RAF/MEK/ERK (MAPK) signaling for tumor cell growth[1]. RAF and MEK inhibitors show remarkable clinical efficacy in BRAF^{V600E} melanoma[2, 3]; however, resistance to these agents remains a formidable challenge[2, 4]. Global characterization of resistance mechanisms may inform the development of more effective therapeutic combinations. Here, we performed systematic gain-of-function resistance studies by expressing >15,500 genes individually in a BRAF^{V600E} melanoma cell line treated with RAF, MEK, ERK, or combined RAF/MEK inhibitors. These studies revealed a cyclic AMP-dependent melanocytic signaling network not previously associated with drug resistance, including G-protein coupled receptors, adenyl cyclase, protein kinase A and cAMP response element binding protein (CREB). Preliminary analysis of biopsies from BRAF^{V600E} melanoma patients revealed that phosphorylated (active) CREB was suppressed by RAF/MEK-inhibition but restored in relapsing tumors. Expression of transcription factors activated downstream of MAP kinase and cAMP pathways also conferred resistance, including c-FOS, NR4A1, NR4A2 and MITF. Combined treatment with MAP kinase pathway and histone deacetylase inhibitors suppressed MITF

expression and cAMP-mediated resistance. Collectively, these data suggest that oncogenic dysregulation of a melanocyte lineage dependency can cause resistance to RAF/MEK/ERK inhibition, which may be overcome by combining signaling- and chromatin-directed therapeutics.

To identify genes whose up-regulation confers resistance to MAPK pathway inhibition, we expressed 15,906 human open reading frames (ORFs)[5] (Extended Data Fig. 1, Supplementary Table 1) in a BRAF[V600E]–mutant, MAPK-pathway dependent melanoma cell line (A375)[6, 7] and determined their effects on sensitivity to small-molecule inhibitors targeting RAF (RAF-i), MEK (MEK-i), ERK[8] (ERK-i) and a combination of RAF and MEK (RAF/MEK-i) (Fig. 1a). In this experiment, 14,457 genes (90.9%, Fig. 1a) passed quality control filters and were evaluated for their effects on drug sensitivity (Extended Data Fig. 2a, b, c). We identified 169 genes (1.16%) whose overexpression conferred resistance to at least one MAPK-pathway inhibitor (Extended Data Fig. 2d).

These screens identified diverse resistance effectors (Fig. 1b), including genes that activate ERK signaling (*KRAS[G12V]*, MEK1[S218/222D], *RAF1, MOS, FGR*, *AXL, FGFR2, SRC* and COT/*MAP3K8*)[6, 9–13] and *RAS*-guanine exchange factors (*RASGRP2, 3* and *4*) (Extended Data Fig. 2d). Previously unrecognized resistance mechanisms were also identified, including modifiers of "stem-ness" (*POU5F4/OCT4*, *NANOG*), ubiquitin pathway components (*KLHL*-family members, *TRIM*-family members) and non-Ras guanine exchange factors (*VAV1*, other *DBS* and *PLEKHG* family members). Furthermore, several ERK-regulated transcription factors emerged, including *FOS, JUNB, ETS2* and *ETV1* (Extended Data Fig. 2c).

To verify resistance effects, we re-expressed each candidate gene in A375 cells and calculated the area under the curve (AUC, Extended Data Fig. 3b) for MAPK-i growth inhibition (GI$_{50}$) assays (Extended Data Fig. 3a). The fraction of candidate genes that were validated ($p < 0.05$) by these experiments ranged from 64.2% (RAF-i) to 84.5% (RAF/MEK-i) (Fig. 2a). Of the 75 RAF-i resistance genes, 71 (94.6%) also imparted resistance to MEK-i and RAF/MEK-i and only 18 (25.4%) of the 71 RAF-i, MEK-i and RAF/MEK-i resistance genes retained sensitivity to ERK-i (Extended Data Fig. 3d, e). Thus, the majority of the genes that confer resistance to single agent RAF-i are resistant to both RAF/MEK-i (94.6%) and ERK-i (70.6%) (Extended Data Fig. 3e, f). Aside from a subset of MAP kinases and tyrosine kinases, most genes produced only minimal p-ERK rescue in the presence of MAPK-i (Extended Data Fig. 3c), consistent with the high degree of ERK inhibitor resistance observed in our validation experiments (Fig. 2a). These data suggest that many resistance mechanisms may circumvent the entire RAF/MEK/ERK module.

We extended our validation studies across seven additional BRAF[V600E] lines (Extended Data Fig. 4a-d). Overall, 110 genes (66.7%) conferred resistance to the query inhibitors in at least 2 of 7 additional BRAF[V600E] melanoma lines (Fig. 2b). Many genes again conferred resistance to all inhibitors/combinations examined (Fig. 2b). Next, we organized resistance genes into mechanistically related classes and identified those that exhibited the most extensive validation across our BRAF[V600E] cell lines (Fig. 2c). Based on these criteria, G-protein coupled receptors (GPCRs) emerged as the top ranked protein class (Extended Data Fig. 4e). Each validated GPCR conferred resistance to all MAPK inhibitors tested (Figs. 2b).

Many GPCRs activate adenyl cyclase (AC), which converts adenosine triphosphate (ATP) to cyclic adenosine monophosphate (cyclic AMP/cAMP)[14], the primary target of which is protein kinase A (PKA). Consistent with these observations, the AC gene *ADCY9* was also identified as a resistance effector (Extended Data Fig. 2d, Extended Data Fig. 4f, g) and the catalytic subunit of PKAα (*PRKACA*) had the highest composite rescue score within the Ser/Thr Kinase class (Fig. 2b, c). Both genes conferred resistance across all MAPK pathway inhibitors examined (Fig. 2b, Extended Data Fig. 4f).

We therefore hypothesized that a signaling network characterized by GPCR activation and AC/cAMP/PKA induction may induce resistance to MAPK inhibitors in melanoma (Fig 4f). This predicted network resembles a growth-essential lineage pathway in primary melanocytes, which require GPCR-mediated cAMP signaling for growth *in vivo*[15]. To test this hypothesis, we determined whether cAMP-mediated signaling was sufficient to confer resistance to MAP kinase pathway inhibitors. Both cAMP and the AC activator forskolin increased intracellular cAMP (Extended Data Fig. 5a) and conferred resistance to all MAPK-pathway inhibitors queried across a panel of cell lines (Fig. 3a, Extended Data Fig. 5b) without affecting baseline cell growth (Extended Data Fig. 5c, d). Forskolin/cAMP resistance was PKA-dependent; it was blocked using the PKA inhibitor H89 (Fig. 3b, Extended Data Fig. 5e). The resistance phenotype was also specific to MAPK-pathway inhibitors (Extended Data Fig. 5f). Thus, cAMP/PKA activation can confer resistance to MAPK pathway inhibition in melanoma cells.

Two well-characterized transcription factor substrates of cAMP/PKA are CREB and ATF1, which regulate the expression of genes whose promoters harbor cyclic AMP response elements (CREs). To determine whether cAMP-mediated resistance may involve a CREB-dependent mechanism, we measured phosphorylation of these proteins following addition of either forskolin or exogenous cAMP. Both agents (Extended Data Fig. 6a, b), as well as most GPCR genes (Fig. 3c, Extended Data Fig. 6c, d), induced CREB and ATF1 phosphorylation, although only a subset of GPCRs increased steady-state intracellular cAMP (Extended Data Fig. 6e). Expression of dominant-negative CREB proteins (CREB[R301L, Ref. 16] or A-CREB[17], Extended Data Fig. 6f) suppressed forskolin-induced resistance to all MAPK-pathway inhibitors tested (Fig. 3d). These results support the hypothesis that cAMP-mediated resistance may operate in large part through a CREB-dependent mechanism, though the roles of other downstream effectors cannot be excluded.

We next assessed the possible contribution of a cAMP/PKA/CREB mechanism in BRAF[V600E] melanoma patients by measuring CREB/ATF1 phosphorylation in tumor biopsies obtained prior to or during treatment and following relapse with vemurafenib alone or dabrafenib and tremetinib in combination (Extended Data Fig. 7a). In contrast to cell lines *in vitro*, CREB/ATF1 phosphorylation was detectable in pre-treatment BRAF[V600E] melanoma biopsy specimens (Fig. 3e, Extended Data Fig. 7b). These results were consistent with the fact that cAMP pathway agonists are excluded from melanoma tissue culture media *in vitro*. Phospho-CREB/ATF1 levels were suppressed in the cohort of patients treated with RAF or RAF/MEK inhibition (Fig. 3e, Extended Data Fig. 7b, c, d). In contrast, the levels of CREB/ATF1 phosphorylation observed in patient cohorts upon tumor relapse were statistically indistinguishable from those detected in the pre-treatment cohort (Fig. 3e).

However, in the single case where matched pre-, on-treatment and post-relapsed samples could be assessed, pCREB/pATF1 levels did not correlate with drug response (Extended Data Fig. 7b). These preliminary clinical results thus raise the possibility that a CREB-dependent mechanism might contribute to resistance to RAF/MEK inhibition in a subset of melanomas.

Based on these clinical findings, we sought to determine if MAPK pathway inhibitors might modulate pCREB/pATF1 *in vitro* when cAMP-dependent signaling is active. We treated BRAF[V600E] melanoma cells with cAMP/IBMX and measured CREB/ATF1 phosphorylation following exposure to MAPK inhibitors. Each MAPK inhibitor partially blunted the increase in pCREB/pATF1 produced by exogenous cAMP (Fig. 3f and Extended Data Fig. 7e), suggesting that cAMP-dependent CREB/ATF1 activity may be reduced by pharmacologic MAPK inhibition.

In melanocytes, oncogenic *BRAF* or *NRAS* can substitute for cAMP signaling[18–20]. We therefore hypothesized that a cAMP-mediated lineage program might mediate resistance by inducing CREB-dependent trans-activation of effectors normally under MAPK control (Fig. 4f). We identified c̲AMP r̲esponse e̲lements (CREs) in the promoters of 19 resistance genes ($p = 5.0 \times 10^{-50}$, Fig. 4a, Extended Data Fig. 8a), of which three lineage-expressed (Extended Data Fig. 8c) transcription factors (TFs)—*MITF*, *FOS* and *NR4A2*—showed high composite resistance scores (z > 50; Extended Data Fig. 8b). *MITF*, *FOS*, *NR4A2* and *NR4A1* (an *NR4A2* homologue and validated resistance gene) showed reduced transcript levels following MEK-i treatment (Fig. 4b). Activating MITF phosphorylation[21, 22] decreased within 1 hour and total MITF protein was undetectable 48–96 hours after MEK inhibition (Extended Data Fig. 9a, b). All four TFs exhibited 2- to 20-fold increases in mRNA expression within 1 hour of forskolin treatment (Fig. 4c) and MITF showed sustained increases in protein expression across multiple melanoma cell lines and MAPK pathway inhibitors (Extended Data Fig. 9c-f). Thus, CREB-responsive transcription factor resistance genes operate downstream of both MAPK- and cAMP–dependent signaling.

To further interrogate connections between cAMP signaling and resistance genes, we employed an expression profiling resource generated by the Library of Integrated Network-based Cellular Signatures (LINCS) program; an extensive catalog of gene-expression profiles collected from human cells following chemical and genetic perturbation. We compared the signatures derived from all candidate resistance genes to a LINCS signature of AC stimulation and found that the genes most similar to the signature of AC activation were enriched for GPCR-pathway associated candidate genes, including GPCRs, PKA and cAMP/MAPK-regulated TFs (Extended Data Fig 9g). Thus, GPCR-pathway related resistance genes and cAMP agonists function to elaborate a common transcriptional output.

Of the genes co-regulated by MAPK and cAMP/CREB, *MITF* was intriguing because of its essential role in melanocyte development[23] and as a melanoma "lineage survival" oncogene[19]. Expression of PKAα, *ADCY9* or a subset of resistance-associated GPCRs enabled sustained MITF expression, even in the setting of MEK-i (Extended Data 9h), thereby confirming that a GPCR/PKA/AC cascade can regulate MITF expression in melanoma cells. Moreover, impairment of MITF protein levels by small hairpin RNA

(shRNA) (Extended Data Fig. 10a, 10b) or co-treatment with a PKA-inhibitor (H89, Extended Data Fig. 10c) blunted forskolin-mediated resistance to MAPK-pathway inhibitors (Fig. 3b, Extended Data Fig. 10a).

In a series of three patient-matched melanoma biopsies obtained over the course of RAF/MEK inhibition, we observed that MITF levels were reduced following initiation of MAPK-i therapy and partially restored in the context of relapse in one patient (Extended Data Fig. 10d), consistent with the notion that aberrant expression of certain cAMP/PKA regulated transcription factors may correlate with resistance in some melanoma patients. Collectively, our findings indicate that resistance-associated transcriptional outputs may be governed by several TFs in melanoma cells.

Our results support a model wherein aberrant signaling from melanocyte lineage pathways may converge on MITF or other TFs to drive resistance to MAPK pathway inhibitors. SOX10 and MITF expression can be impaired following treatment with histone deacetylase inhibitors (HDAC-i), though these agents do not act exclusively through SOX10/MITF[24]. We hypothesized that combined HDAC/MAPK inhibition might prevent cAMP/MITF-driven resistance in melanoma cells. Indeed, multiple HDAC inhibitors (panobinostat/ LBH589, vorinostat/SAHA and entinostat/MS275) reduced both SOX10 and MITF expression (Extended Data Fig. 10e), even in the presence of forskolin (Fig. 4d, Extended Data Fig. 10f). Each of these HDAC inhibitors reversed cAMP-mediated resistance to MAPK-pathway inhibition *in vitro* (Fig. 4e). Of note, forced expression of MITF did not abrogate HDAC-i sensitivity, indicating that the HDAC-i growth inhibitory effects do not act solely through this mechanism (Extended Data Fig. 10g). Nonetheless, these results raise the possibility that addition of HDAC inhibitors to combined RAF/MEK inhibition might offer a novel clinical strategy to achieve more durable control of some BRAF^{V600E} melanomas.

The clinical benefit of RAF/MEK-i therapy in BRAF^{V600E} melanoma remains temporary, and resistance mechanisms are incompletely understood. The GPCR/cAMP/AC/PKA/CREB module identified here is highly reminiscent of lineage survival signaling in melanocytes. Our results and those of other groups[25, 26] suggest that this lineage dependency may become reactivated as part of a clinical mechanism of resistance to RAF/MEK inhibition (Fig. 4f) and are bolstered by recent studies showing that MITF transcriptional targets are up regulated during the course of treatment with MAPK-pathway inhibitors[27]. The application of genome-scale functional approaches to characterize anticancer drug resistance, together with directed experimental and clinical studies, may offer a general framework for discovery and clinical prioritization of novel therapeutic regimens.

Methods Summary

The arrayed ORF screens were performed as previously described[6] using the Center for Cancer Systems Biology/Broad Institute Lentiviral Expression Library[5]. Effects of individual ORFs on drug sensitivity were determined by measuring differential viability (ratio of raw viability in MAPK-pathway inhibitor to viability in DMSO) and subsequently normalized across plates using a z-score/standard score. Secondary screens to prioritize

identified resistance candidates were performed in eight BRAF[V600]-mutant melanoma cell lines in a manner similar to the primary screens. Prioritization of candidates was accomplished by generation of a composite rescue score for each gene, representing the extent and breadth of ORF-induced resistance phenotype across cell lines. Further validation and characterization of candidate resistance genes and pathways were accomplished using both biochemical and cell biological approaches. Detailed descriptions of all procedures are included in Methods.

Experimental Methods

Broad-Institute/Center for Cancer Systems Biology Lentiviral Expression Library

The genesis, cloning, sequencing and production of the Broad-Institute/Center for Cancer Systems Biology Lentiviral Expression Library have been described previously[5]. All ORFs described in this manuscript were expressed from pLX304 (http://www.addgene.org/25890), a lentiviral expression vector that encodes a C-terminal V5-epitope tag, a blasticidin resistance gene and drives ORF expression from a CMV-promoter. All clones described in this manuscript are publicly available via members of the ORFeome collaboration (http://www.orfeomecollaboration.org/).

Genome scale ORF resistance screens

A375 were robotically seeded into 384-well white walled, clear-bottom plates in RPMI-1640 (cellgro) supplemented with 10% FBS and 1% Penicillin/Streptomycin. The Broad-Institute/Center for Cancer Systems Biology Lentiviral Expression Library[5] was arrayed on 47×384 well plates, from which virus was robotically transferred to cell plates. Cell plates were randomly divided into 6 treatment arms in duplicate: DMSO, PLX4720, AZD6244, PLX4720+AZD6244, VRT11e or a parallel selection arm (blasticidin). Twenty-four hours after seeding, polybrene was added directly to cells (7.5 μg/ml final concentration), followed immediately by robotic addition of the CCSB/Broad Institute virus collection (3 μL/well) and centrifuged at 2250 RPM (1,178×g) for 30 min. at 37° C. Following a 24 hr. incubation at 37° C (5% CO_2), media and virus was aspirated and replaced with complete growth media or media containing blasticidin (10 μg/ml) to select for ORF expressing cells and to determine infection efficiency. Forty-eight hours after media change, unselected (no blasticidin) cells were treated with DMSO (vehicle control) or MAPK pathway inhibitors to a final concentration of 2 μM (PLX4720, VRT11e) or 200 nM (AZD6244). Identical concentrations used for single agent PLX4720 and AZD6244 treatment were used for combined PLX4720/AZD6244 treatment. Single-agent inhibitors were balanced with DMSO such that all wells contained 0.033% DMSO. Four days (96 hrs.) after drug addition, cell viability was assessed via robotic addition of CellTiterGlo (1:6 dilution) followed by 10 min. orbital agitation at room temperature and subsequent quantification (EnVision Multilabel Reader, Perkin Elmer). Primary screens were performed in 16 individual batches in which 2–3 viral stock plates were screened per batch against all compounds.

Identification of resistance candidates from primary screening data

Following quantification of cell viability, duplicate luminescence values were averaged for each ORF within each treatment condition. Percent rescue capability of each ORF was determined by dividing the average luminescence value in drug by the average luminescence value in DMSO. Subsequent percent rescue values were normalized within screening plates using the plate average and standard deviation to generate a z-score/standard score of percent rescue.

To calculate infection efficiency of each ORF, luminescence values in the presence of blasticidin were normalized to the average luminescence in DMSO and expressed as a percentage. ORF-mediated effects on cell viability in the absence of drug were assessed by taking the average luminescence value for each ORF in DMSO and normalizing each value to the plate average and standard deviation (z-score).

To identify candidate resistance genes, we first filtered out all wells that had an infection efficiency of less than 65%. To eliminate genes with significant effects on cellular growth in the absence of drug treatment, we then filtered out genes that had a z-score in DMSO of greater than 2.0 or less than –2.0. We additionally eliminated wells from further analysis that showed a replicate variability (in DMSO) of greater than 29.15% (equivalent to >2 standard deviations from the average replicate variability). Following this initial filtering, 14, 457 genes remained for subsequent analysis. Within each drug treatment condition, wells showing replicate variability of >2 standard deviations from the mean variability per drug were eliminated from further analysis. Finally, genes showing a z-score of percent rescue of greater than 2.5 were nominated as resistance gene candidates.

Neutral control genes (19) were nominated from primary screening data by identifying genes across virus plates and screening batches with 1) high infection efficiency (>98.5%), 2) minimal effects on baseline cell growth (z-score of viability in DMSO between –0.5 to 0.5) and 3) a rescue score (z-score of percent rescue) < 0.25 (e.g. no effect on drug sensitivity or resistance). DNA encoding candidates (169), negative controls (eGFP, n=9; HcRed, n=15; Luciferase, n=16) positive controls (MEK1[DD], KRAS[G12V], *MAP3K8*/COT) and neutral controls (19) were isolated from the CCSB/Broad expression collection and used to create a validation viral stock distinct from that used in the primary screens.

Drug sensitivity curves in A375 expressing candidate ORFs

A375 were seeded, infected and drug treated exactly as in primary screens using 4 μl of validation viral stock and concentrations of inhibitors ranging from 10 μM to 100 nM in half-log increments. For combinatorial PLX4720/AZD6244 treatment, a fixed dose of PLX4720 (2 μM) was combined with AZD6244 in doses ranging from 10 μM to 100 nM in half-log increments. Viability was assessed as in the primary screen. Resulting luminescence for each ORF was normalized to luminescence in DMSO (% rescue) for each drug and drug concentration. Resulting sensitivity curves for each ORF were log transformed and the area under the curve (AUC) calculated using Prism GraphPad software. Resulting AUC for each candidate and control ORF/drug combination were normalized to that of the negative and

neutral controls using a z-score (described above). ORFs yielding a z-score of >1.96 (*p < 0.05*) were considered to be validated candidates in this cell line.

Validation screens in additional BRAF^{V600E} cell lines

Validation screening in additional BRAF^{V600E} melanoma cell lines was performed exactly as in the primary screen, but cell lines were empirically optimized for seeding density and viral dilution. Due to sensitivity of these cell lines to polybrene and virus exposure, all cell lines except for WM266.4 were treated with polybrene and virus, spun for 1 hr. at 2250 RPM (1,178×*g*) followed immediately by complete virus/media removal and change to complete growth media. WM266.4 were treated with polybrene and virus, spun for 30 min. at 2250 RPM (1,178×*g*) and incubated for 24 hours before virus/media removal and change to complete growth media 24 hours after infection. For experimental determination of infection efficiency, blasticidin (5 μg/ml) was added 24 hrs. after media change. All drug treatments and viability measurements were performed as in primary screens.

Resulting luminescence values were normalized to DMSO (percent of DMSO or 'percent rescue'). The resulting percent rescue was normalized to the mean and standard deviation of all negative and neutral controls to yield a z-score of percent rescue. Genes with a z-score of percent rescue of >4 in at least two instances were considered to have validated. "Composite rescue scores" were derived by summing the z-score of percent rescue of each gene across all drugs and cell lines. Average composite rescue scores for each protein class were generated by taking the average composite rescue score of all genes within a given protein class.

pERK and V5 immunoassays

For analysis of ERK phosphorylation, A375 were seeded at 1500 cells/well in black walled, clear bottomed, 384-well plates, virally transduced with all candidates and controls and treated with PLX4720, AZD6244 and combinatorial PLX4720/AZD6244 exactly as in the primary resistance screens. Eighteen hours after drug treatment, media was removed and cells were fixed with 4% formaldehyde and 0.1% Triton X-100 in PBS for 30 minutes at room temperature. Following removal of fixation solution, cells were washed once with PBS and blocked in blocking buffer (LiCOR) for 1 hour at room temperature with shaking. After removal of blocking buffer, fixed cells were incubated with primary antibody against ERK phosphorylated at Thr202/Tyr204 (Sigma, #M8159, 1:2000) in LiCOR blocking buffer containing 0.1% Tween-20 and for 18 hours at 4 °C with shaking. Antibody was removed and wells were washed thrice with 0.1% Tween-20 in water followed by incubation in secondary antibody (IRDye 800CW LiCOR, 1:1,200) and dual cellular stains, including Sapphire700 (LiCOR, 1:1000) and DRAQ5 (Cell Signaling Technology, 1:10,000), all diluted in LiCOR blocking buffer (no detergent) and incubated for 1 hour at room temperature with shaking. Secondary antibody/cell stain was removed and washed thrice with 0.1% Tween-20 in water followed by a single wash in PBS. PBS was removed and plates were dried for 10 minutes at room temperature in the dark followed immediately by imaging on an Odyssey CLx Infrared Scanner. For pERK and cellular stain, background was calculated based on signal observed in control wells containing only secondary antibody in blocking buffer and subtracted from each experimental well. Total pERK signal was

normalized to total cellular stain for each ORF in each drug condition. The resulting values were subsequently normalized to DMSO (percent of DMSO) for each ORF per drug condition

V5 immunostaining for ectopic ORF expression was performed as described for the ERK phosphorylation assay, above. Briefly, cells were seeded at 3000–4000 cells/well and infected in parallel to validation screens. Seventy-two hours after infection, cells were fixed, blocked and stained as described for the pERK assay, instead using an antibody directed against the V5 epitope (Invitrogen, #R96025, 1:5,000, Invitrogen). Subsequent washes, secondary antibody incubations and total cellular staining protocol were identical to those described for the pERK assay, above. V5 and cellular stain (DRAQ5/Sapphire700) intensity were quantified as above, background signal subtracted (determined by signal intensity in uninfected wells with no V5 epitope and stained with secondary antibody, only) and V5 signal intensity normalized to cellular stain intensity.

Detection of GPCR-mediated cyclic AMP production

HEK293T cells were seeded at a density of 2.5×10^5 cells/well in 12-well plates. Twenty-four hours after seeding, cells were transfected with 250 ng of the indicated ORF (pLX304 expression vector) using 3 μl of Fugene6 (Promega) transfection reagent. Forty-seven hours after transfection, cells were treated either with DMSO (1:1000) or IBMX (30 μM). In addition, forskolin (10 μM) and 100 M IBMX were added as positive controls for indicated time. Cells were subsequently lysed in triton x-100 lysis buffer (Cell Signaling Technology) and resulting lysates split for cAMP ELIZA (Cell Signaling Technology, #4339) or parallel western blot analysis. cAMP ELIZA was performed exactly per the manufacturers recommended protocol. Following quantification the inverse absorbance was calculated and normalized to that of negative control ORFs.

Identification of Cyclic AMP Response Elements in candidate resistance genes

Gene sets that share a common *CREB1*, *ATF1*, *ATF2* or *JUN* DNA response element within +/− 2 kb of their transcriptional start site (as defined by TRANSFAC, version 7.4, http://www.gene-regulation.com/) were identified and downloaded from the MSigDB website (Extended Data Fig. 8a), available at http://www.broadinstitute.org/gsea/msigdb). CRE-containing genes present in individual gene sets were subsequently identified within the group of screened ORFs and within the group of candidate/neutral control ORFs. The ratio of CRE-containing genes to screened genes (expected) was compared to the ratio of CRE-containing genes to candidate/neutral control genes (actual) across gene sets. A *p* value for the observed enrichment of CRE-containing genes in the candidate genes over the expected representation within the screening set was calculated using Pearson's chi-squared test.

Cell lines and reagents

A375, SKMEL28, SKMEL19, UACC62, COLO-679 and WM983b were all grown in RPMI-1640 (Cellgro), 10% FBS and 1% penicillin/streptomycin. WM88, G361, SKMEL5, WM266.4, COLO-205 and 293T were all grown in DMEM (Cellgro), 10% FBS and 1% penicillin/streptomycin. All cell lines were acquired via the Cancer Cell Line Encyclopedia (http://www.broadinstitute.org/ccle/home) except for SKMEL19, which was a generous gift

of Dr. Neal Rosen, Memorial Sloan-Kettering Cancer Center, NY, NY). AZD6244 (PubChem ID: 10127622) was purchased from Selleck Chemicals, PLX4720 (PubChem ID: 24180719) was purchased from Symansis and VRT11e was synthesized by contract based on its published structure[8]. Forskolin, IBMX (3-Isobutyl-1-methylxanthine) and α-MSH (α-melanocyte stimulating hormone) were purchased from Sigma. Panobinostat/LBH-589 was purchased from BioVision, Vorinostat/SAHA and Entinostat/MS-275 from were purchased from Cayman Chemical. All small molecules were dissolved in DMSO.

Pharmacologic Growth Inhibition Assays

Melanoma cell lines were seeded into 384-well, white-walled, clear bottom plates at the following densities; A375, 500 cells/well; SKMEL19, 1500 cells/well; SKMEL28, 1000 cells/well; UACC62, 1000 cells/well;, WM266.4, 1800 cells/well; G361, 1200 cells/well, COLO-679, 2000 cells/well; SKMEL5, 2000 cells/well; WM983b 1500 cells/well, WM88 1800 cells/well; COLO-205 1500 cells/well). Twenty-four hours after seeding, serial dilutions of the relevant compound were prepared in DMSO to 1000x stocks. Drug stocks were then diluted 1:100 into appropriate growth media and added to cells at a dilution of 1:10 (1x final), yielding drug concentrations ranging from 100 μM to 1×10^{-5} μM, with the final volume of DMSO not exceeding 1%. When indicated, forskolin (10 μM), IBMX (100 μM), dbcAMP (100 μM) were added concurrent with MAPK-pathway inhibitors. Cells were incubated for 96 h following addition of drug. Cell viability was measured using CellTiterGlo viability assay (Promega). Viability was calculated as a percentage of control (DMSO treated cells). A minimum of six replicates were performed for each cell line and drug combination. Data from growth-inhibition assays were modeled using a nonlinear regression curve fit with a sigmoid dose–response. These curves were displayed and GI_{50} generated using GraphPad Prism 5 for Windows (GraphPad). Sigmoid-response curves that crossed the 50% inhibition point at or above 1.0 μM or 10.0 μM have GI_{50} values annotated as >1.0 μM or >10.0 μM, respectively. For single-dose studies, WM266.4 were seeded at 5,000 cells/well in 96-well, white-walled, clear bottom plates and the identical protocol (above) was followed, using a single dose of indicated drug.

ORF and shRNA expression methods for experimental studies

Indicated ORFs were expressed from pLX-304 (Blast, V5) lentiviral expression plasmids, whereas shRNAs were expressed from pLKO.1. shRNAs and controls are available through The RNAi Consortium Portal (http://www.broadinstitute.org/rnai/public/) and are identifiable by their sequence and clone ID: shLuc (CTTCGAAATGTCCGTTCGGTT, TRCN0000072243), shMITF_492 (TTAGCCTAGAATCAAGTTATA, TRCN0000329869) and shMITF_573 (CGGGAAACTTGATTGATCTTT, TRCN0000019123). For lentiviral production, 293T cells (1.0×10^6 cells/ 6-cm dish) were transfected with 1 μg of pLX-Blast-V5-ORF or pLKO.1-shRNA, 900 ng 8.9 (gag, pol) and 100 ng VSV-G using 6 μl Fugene6 transfection reagent (Promega). Viral supernatant was harvested 72 h post-transfection. WM266.4 were infected at a 1:10–1:20 dilution (ORFs) or 1:100 dilution (shRNA) of virus in 6-well plates (2.0×10^5 cells/ well, for immunoblot assays) or 96-well plates (3.0×10^3, for cell growth assays) in the presence of 5.5 μg/ml polybrene and centrifuged at 2250 RPM for 60 min. at 37∘ C followed immediately by removal of media and replacement with complete

growth media. Seventy-two hours after infection, drug treatments/pharmacological perturbations were initiated (see below).

Generation of *CREB1* and A-CREB reagents

Wild-type CREB1 (Isoform B, NM_134442.3) was obtained through the Broad Institute RNAi Consortium, a member of the ORFeome Collaboration (http://www.orfeomecollaboration.org/). Arginine 301 of CREB was mutated to Leucine yielding CREB^{R301L}(equivalent to CREB^{R287L} in isoform A) using the QuikChange Lightning Mutagenesis Kit (Agilent), performed in pDonor223 (Invitrogen). CREB^{R301L} was transferred into pLX304 using LR Clonase (Invitrogen) per manufacturer's recommendation. The A-CREB cDNA[17] was synthesized (Genewiz) with flanking Gateway recombination sequences, recombined first into pDonor223 and subsequently into pLX304 as described for *CREB1* mutant cDNAs.

Quantitative RT/PCR

mRNA was extracted from WM266.4 using the RNeasy kit (Qiagen) and homogenized using the Qiashredder kit (Qiagen). Total mRNA was used for subsequent reverse transcription using the SuperScript III First-Strand Synthesis SuperMix (Invitrogen). 5 µl of reverse-transcribed cDNA was used for quantitative PCR using SYBR Green PCR Master Mix and gene-specific primers, in quadruplicate, using an ABI PRISM 7900 Real Time PCR System. Primers used for detection were as follows; *NR4A2* forward: 5'- GTT CAG GCG CAG TAT GGG TC -3'; *NR4A2* reverse: 5'- AGA GTG GTA ACT GTA GCT CTG AG -3'; *NR4A1* forward: 5'- ATG CCC TGT ATC CAA GCC C -3'; *NR4A1* reverse: 5'- GTG TAG CCG TCC ATG AAG GT -3'; *DUSP6* forward: 5'- CTG CCG GGC GTT CTA CCT -3'; *DUSP6* reverse: 5'- CCA GCC AAG CAA TGT ACC AAG -3'; *MITF* forward: 5'- TGC CCA GGC ATG AAC ACA C-3'; *MITF* reverse: 5'- TGG GAA AAA TAC ACG CTG TGA G -3'; *FOS* forward: 5'- CAC TCC AAG CGG AGA CAG AC -3'; *FOS* reverse: 5'- AGG TCA TCA GGG ATC TTG CAG -3'; *TBP* forward: 5'- CCC GAA ACG CCG AAT ATA ATC C -3'; *TBP* reverse: 5'- GAC TGT TCT TCA CTC TTG GCT C -3'. Relative expression was determined using the comparative CT method (Applied Biosystems) followed by normalization to the DMSO/T$_0$ time point.

Immunoblots and antibodies

Adherent cells were washed once with ice-cold PBS and lysed passively with 1% NP-40 buffer [150 mM NaCl, 50 mM Tris pH 7.5, 2 mM EDTA pH 8, 25 mM NaF and 1% NP-40] containing 2x protease inhibitors (Roche) and 1x Phosphatase Inhibitor Cocktails I and II (CalBioChem). Lysates were quantified (Bradford assay), normalized, reduced, denatured (95 °C) and resolved by SDS gel electrophoresis on 4–20% Tris/Glycine gels (Invitrogen). Resolved protein was transferred to nitrocellulose or PVDF membranes, blocked in LiCOR blocking buffer and probed with primary antibodies recognizing MITF (NeoMarkers, Clone C5, #MS-771-P, 1:400), Cyclin D1 (NeoMarkers, Clone Ab-3, #RB-010-P, 1:400), pERK1/2 (Thr202/Tyr204, Sigma, #M8159, 1:5,000), SLVR (Sigma, SAB4100050, 1:500), vinculin (Sigma, V9131, 1:20,000), total MEK1 (BD Transduction, #610122, 1:1000), acetylated histone H3 (Millipore, #06-599, 1:2000) and V5 epitope (Invitrogen, #R96025,

1:5,000). The following antibodies were purchased from Cell Signaling Technology and used at 1:1000 dilution: pMEK1/2 (Ser217/221, #9154), FOS (#2250), pCREB/pATF1 (Ser133, Ser63, respectively, #9196), CREB (#4820) and β-Actin (#3700, 1:20,000). The following antibodies were purchased from Santa Cruz Biotechnology: BCL2 (Clone C-2, sc-7382, 1:250), TRP1 (Clone G-17, sc-10443, 1:1000), Melan-A (Clone A103, sc-20032, 1:1000), ERK2 (Clone C-14, sc-154, 1:5,000), NR4A1/Nur77 (Clone M-210, sc-5569, 1:250), NR4A2/Nurr1 (Clone N-20, sc-991, 1:500), SOX10 (Clone N-20, sc-17342, 1:400). After incubation with the appropriate secondary antibody (anti-rabbit, anti-mouse or anti-goat IgG, IRDye-linked; 1:15,000 dilution; IRDye 800CW, 1:20,000 IRDye 680LT, LiCOR), proteins were imaged and quantified using an Odyssey CLx scanner (LiCOR). Lysates from tumor and matched normal skin were generated by homogenization of tissue in 1% Triton X-100, 50mM HEPES, pH 7.4, 150mM NaCl, 1.5mM MgCl2, 1mM EGTA, 100mM NaF, 10mM Na pyrophosphate, 1mM Na3VO4, 10% glycerol, containing freshly added protease and phosphatase inhibitors (Roche Applied Science Cat. # 05056489001 and 04906837001, respectively). Subsequent normalization and immunoblots were performed as above.

LINCS analysis

To explore transcriptional connections between cAMP signaling and GPCR-pathway associated drug resistance candidates, we expressed all of our candidate and control genes in A375 (as described in "Validation screens in additional BRAFV600E cell lines", above) and generated gene expression profiles using a high-throughput Luminex bead-based platform. We queried the LINCS database (www.lincscloud.org) using a gene-expression signature of adenyl cyclase (AC) stimulation generated by treating A375 cells with colforsin, an AC agonist. We computed the similarity of the colforsin signature to 8729 treatment signatures in the A375 cell line (including the resistance candidate genes) that were available in the database, using a two-tailed weighted enrichment metric (connectivity score). We obtained a ranked list of the treatments based on the strength of the connectivity scores, and examined the ranks of the resistance candidate genes as well as the ranks of neutral control genes.

Expression profiling of melanoma cancer cell lines

We carried out oligonucleotide microarray analysis using the GeneChip Human Genome U133 Plus 2.0 Affymetrix expression array (Affymetrix, Santa Clara, CA). Samples were converted to labeled, fragmented, cRNA per the Affymetrix protocol for use on the expression microarray. All expression arrays are available on the Broad-Novartis Cancer Cell Line Encyclopedia data portal at http://www.broadinstitute.org/ccle/home or on the Gene Expression Omnibus (GSE36133).

Melanoma tumor biopsies

Biopsied tumor material consisted of discarded and de-identified tissue that was obtained with informed consent and characterized under IRB protocol 11–181 (Dana-Farber Cancer Institute). For paired specimens, 'on-treatment' samples were collected 10–14 days after initiation of MAPK inhibitor treatment (Extended Data Fig. 7e).

Acknowledgments

References

1. Solit DB, et al. BRAF mutation predicts sensitivity to MEK inhibition. Nature. 2006; 439:358–362. [PubMed: 16273091]

2. Chapman PB, et al. Improved survival with vemurafenib in melanoma with BRAF V600E mutation. N Engl J Med. 2011; 364:2507–2516. [PubMed: 21639808]

3. Flaherty KT, et al. Combined BRAF and MEK inhibition in melanoma with BRAF V600 mutations. N Engl J Med. 2012; 367:1694–1703. [PubMed: 23020132]

4. Flaherty KT, et al. Improved survival with MEK inhibition in BRAF-mutated melanoma. N Engl J Med. 2012; 367:107–114. [PubMed: 22663011]

5. Yang X, et al. A public genome-scale lentiviral expression library of human ORFs. Nat Methods. 2011; 8:659–661. [PubMed: 21706014]

6. Johannessen CM, et al. COT drives resistance to RAF inhibition through MAP kinase pathway reactivation. Nature. 2010; 468:968–972. [PubMed: 21107320]

7. Wood KC, et al. MicroSCALE screening reveals genetic modifiers of therapeutic response in melanoma. Science signaling. 2012; 5:rs4. [PubMed: 22589389]

8. Aronov AM, et al. Structure-guided design of potent and selective pyrimidylpyrrole inhibitors of extracellular signal-regulated kinase (ERK) using conformational control. J Med Chem. 2009; 52:6362–6368. [PubMed: 19827834]

9. Crews CM, Alessandrini A, Erikson RL. The primary structure of MEK, a protein kinase that phosphorylates the ERK gene product. Science. 1992; 258:478–480. [PubMed: 1411546]

10. Girotti MR, et al. Inhibiting EGF receptor or SRC family kinase signaling overcomes BRAF inhibitor resistance in melanoma. Cancer discovery. 2012

11. Kyriakis JM, et al. Raf-1 activates MAP kinase-kinase. Nature. 1992; 358:417–421. [PubMed: 1322500]

12. Patriotis C, Makris A, Chernoff J, Tsichlis PN. Tpl-2 acts in concert with Ras and Raf-1 to activate mitogen-activated protein kinase. Proc Natl Acad Sci U S A. 1994; 91:9755–9759. [PubMed: 7937886]

13. Pham CD, Arlinghaus RB, Zheng CF, Guan KL, Singh B. Characterization of MEK1 phosphorylation by the v-Mos protein. Oncogene. 1995; 10:1683–1688. [PubMed: 7731726]

14. Pierce KL, Premont RT, Lefkowitz RJ. Seven-transmembrane receptors. Nature reviews. Molecular cell biology. 2002; 3:639–650.

15. Hayward NK. Genetics of melanoma predisposition. Oncogene. 2003; 22:3053–3062. [PubMed: 12789280]

16. Walton KM, Rehfuss RP, Chrivia JC, Lochner JE, Goodman RH. A dominant repressor of cyclic adenosine 3',5'-monophosphate (cAMP)-regulated enhancer-binding protein activity inhibits the cAMP-mediated induction of the somatostatin promoter in vivo. Molecular endocrinology. 1992; 6:647–655. [PubMed: 1350057]

17. Ahn S, et al. A dominant-negative inhibitor of CREB reveals that it is a general mediator of stimulus-dependent transcription of c-fos. Mol Cell Biol. 1998; 18:967–977. [PubMed: 9447994]

18. Dumaz N, et al. In melanoma, RAS mutations are accompanied by switching signaling from BRAF to CRAF and disrupted cyclic AMP signaling. Cancer Res. 2006; 66:9483–9491. [PubMed: 17018604]

19. Garraway LA, et al. Integrative genomic analyses identify MITF as a lineage survival oncogene amplified in malignant melanoma. Nature. 2005; 436:117–122. [PubMed: 16001072]

20. Jane-Valbuena J, et al. An oncogenic role for ETV1 in melanoma. Cancer Res. 2010; 70:2075–2084. [PubMed: 20160028]

21. Hemesath TJ, Price ER, Takemoto C, Badalian T, Fisher DE. MAP kinase links the transcription factor Microphthalmia to c-Kit signalling in melanocytes. Nature. 1998; 391:298–301. [PubMed: 9440696]

22. Wu M, et al. c-Kit triggers dual phosphorylations, which couple activation and degradation of the essential melanocyte factor Mi. Genes Dev. 2000; 14:301–312. [PubMed: 10673502]

23. Hodgkinson CA, et al. Mutations at the mouse microphthalmia locus are associated with defects in a gene encoding a novel basic-helix-loop-helix-zipper protein. Cell. 1993; 74:395–404. [PubMed: 8343963]

24. Yokoyama S, et al. Pharmacologic suppression of MITF expression via HDAC inhibitors in the melanocyte lineage. Pigment Cell Melanoma Res. 2008; 21:457–463. [PubMed: 18627530]

25. Haq R, et al. BCL2A1 is a lineage-specific antiapoptotic melanoma oncogene that confers resistance to BRAF inhibition. Proc Natl Acad Sci U S A. 2013; 110:4321–4326. [PubMed: 23447565]

26. Smith MP, et al. Effect of SMURF2 targeting on susceptibility to MEK inhibitors in melanoma. Journal of the National Cancer Institute. 2013; 105:33–46. [PubMed: 23250956]

27. Frederick DT, et al. BRAF Inhibition Is Associated with Enhanced Melanoma Antigen Expression and a More Favorable Tumor Microenvironment in Patients with Metastatic Melanoma. Clinical cancer research : an official journal of the American Association for Cancer Research. 2013
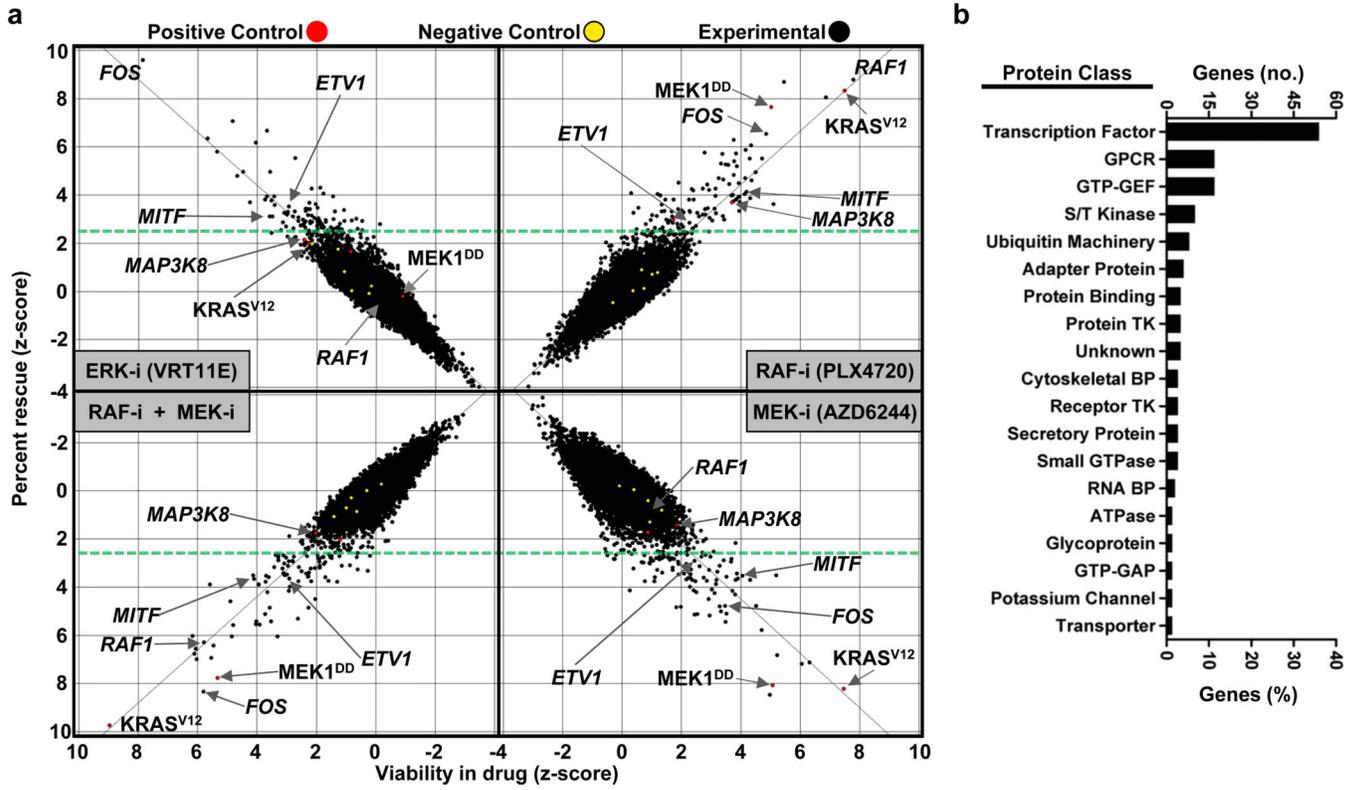
Figure 1. Near genome-scale functional rescue screens for resistance to RAF, MEK and ERK inhibitors

a, A375 cells transduced with the lentiviral expression library were treated in duplicate (technical) with indicated inhibitors and assayed for viability in the presence of compound alone (x-axis) and viability in compound relative to DMSO (y-axis). Values are presented as a z-score. Genes (n=169) with z-scores 2.5 (green dashed line) were nominated as candidate resistance genes. b, Summary of protein classes of candidate-genes identified in primary drug resistance screens. Only protein classes containing 2 genes are shown.

Figure 2. Candidate resistance genes segregate into validating protein classes

a, Area under the curve (AUC) was calculated for MAPK-i drug sensitivity curves in A375 expressing candidate and control genes. Data is presented as a z-score (y-axis), relative to the AUC of all control genes across each MAPK-i.

b, Seven BRAF[V600E]-malignant melanoma cell lines expressing the indicated candidate/control genes were assayed in technical duplicate for viability following treatment with indicated MAPK-i. Cellular viability is presented as a z-score relative to control genes. Genes with a z-score 4 in 2 conditions (drug or cell line) are shown.

c, The strength of the resistance phenotype for each candidate and control gene across all MAPK-i and cell lines is quantified and presented as a composite rescue score.

Figure 3. A cyclic AMP signaling network mediates resistance to RAF, MEK and ERK inhibitors

a, Average fold change (relative to DMSO) in MAPK-i GI_{50} or AUC in a panel of $BRAF^{V600}$-mutant cell lines treated with vehicle (DMSO), forskolin and IBMX (FSK/I) or dbcAMP and IBMX (cAMP/I). n=8 technical replicates, representative of 3 independent experiments.

b, Heat map showing relative cell viability (percent of DMSO) following treatment with forskolin and IBMX (FSK/I) or dbcAMP and IBMX (cAMP/I) in the presence of vehicle (DMSO), the PKA inhibitor H89 and a single dose of indicated MAPK-i.

c, Immunoblot analysis of phosphorylated CREB/ATF1(Ser133/Ser63) in lysates from WM266.4 virally transduced with the indicated expression constructs.

d, Viability of WM266.4 expressing either LacZ (control) or dominant-negative CREB alleles ($CREB^{R301L}$ or A-CREB) following treatment with forskolin and IBMX (FSK/I) in the presence indicated MAPK-i. Viability is expressed as a percentage of DMSO. Error bars

represent s.d. of mean, n=6 technical replicates, representative of two independent experiments.

e, Quantification of pCREB and pATF1 expression following immunoblot analysis of lysates extracted from BRAF^{V600}-mutant human tumors. Tumors were biopsied pre-initiation of treatment (P, n=5), following 10–14 days of MAPK-inhibitor treatment (on-treatment, O, n=6) or following relapse (R, n=7). MAPK-inhibitor therapy is noted. All available samples were tested and reported. Pre-treatment and on-treatment samples are paired. * *p<0.05*, 1-tailed T-Test on treatment cohorts, which may not directly inform responses in individual patient samples.

f, Immunoblot analysis of lysates from WM266.4 following treatment with forskolin and IBMX (FSK/I) or dbcAMP and IBMX (cAMP/I) in the presence of indicated MAPK-i. Quantification of pCREB relative to CREB is shown.

Figure 4. Candidate resistance genes are transcriptional effectors of the MAPK and cAMP-pathways

a, Schematic outlining the identification of candidate resistance genes endogenously regulated by cAMP.

b, Quantification of *TBP*-normalized mRNA levels using real-time quantitative PCR (relative to DMSO-treatment) following a time course of MEK-i treatment. Error bars represent s.d. of mean, n=3 technical replicates representative of 3 independent experiments.

c, Quantification of *TBP*-normalized mRNA levels using real-time quantitative PCR (relative to DMSO-treatment) following treatment with forskolin and IBMX (FSK/I) for the indicated times in the presence of vehicle (DMSO) or MEK-i. Error bars represent s.d. of mean, n=3 technical replicates representative of 2 independent experiments.

d, Immunoblot analysis of lysates from WM266.4 treated with DMSO or MEK-i followed by treatment with panobinostat, vorinostat or entinostat and subsequently stimulated with forskolin and IBMX (FSK/I).

e, Cellular viability of WM266.4 treated with the indicated combinations of MAPK-i, HDAC-i and forskolin and IBMX (FSK/I). Cell viability is shown as a percent of DMSO in un-stimulated/non drug-treated cells. Error bars represent s.d. of mean, n=6 technical replicates representative of 2 independent experiments.

f, A mechanistic model of GPCR-mediated resistance.

Extended Data Figure 1. A systematic, functional approach to identifying drug resistance genes
Schematic outlining the experimental approach taken to identify membrane-to-nucleus
signaling pathways that mediate resistance to MAPK-pathway inhibitors. Resulting data
were used to identify gene networks capable of mediating drug resistance.
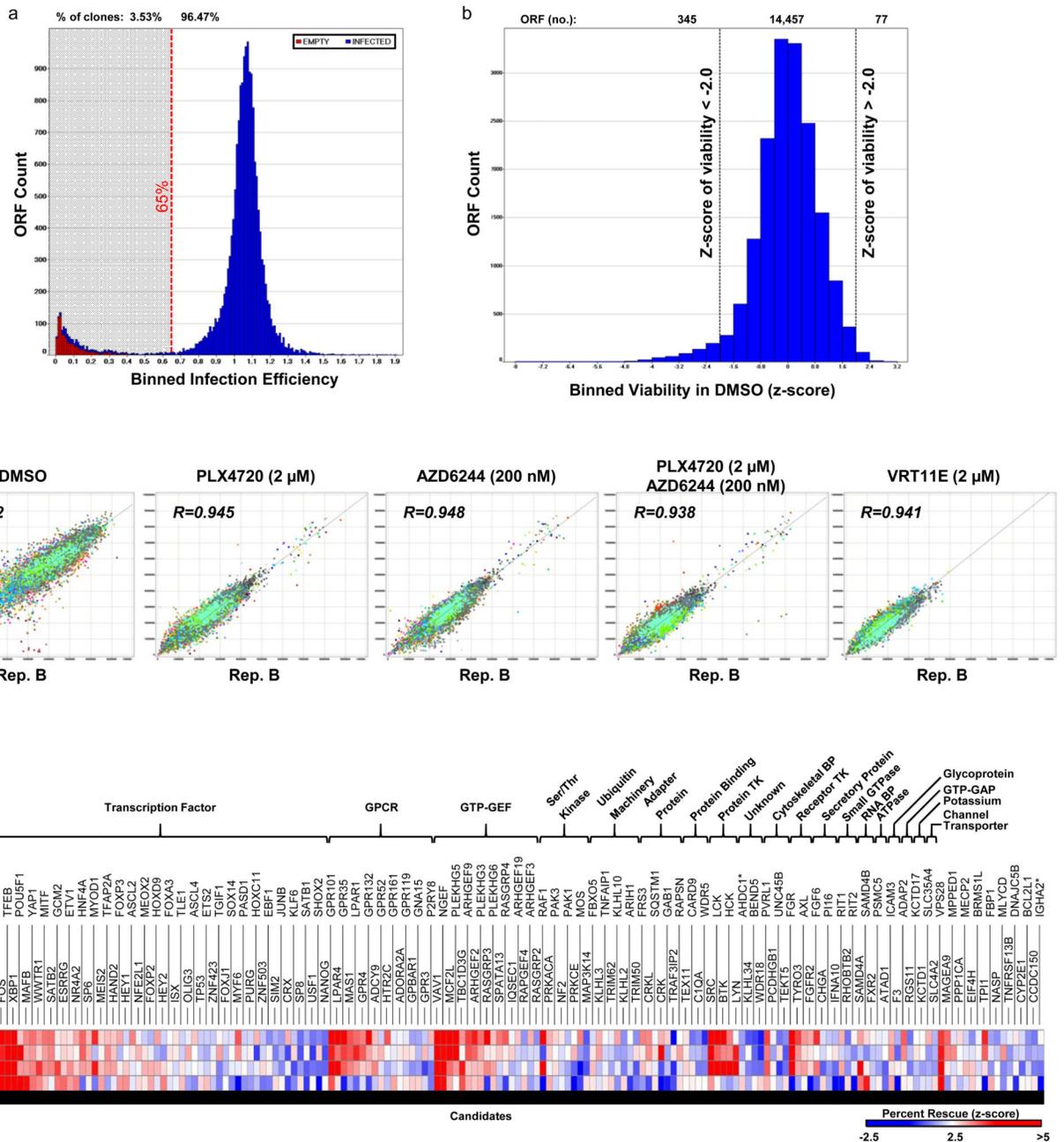
Extended Data Figure 2. Near genome-scale ORF/cDNA screens identify candidate MAPK-pathway inhibitor resistance genes

a, Histogram of infection efficiency in A375 observed in the primary resistance screens. Percent of total ORFs above and below 65% infection efficiency are noted (red, dashed line). **b**, Histogram of the z-score of A375 viability in DMSO observed in the primary resistance screen. Total ORFs above, below and within the indicated z-score thresholds are noted. **c**, Scatter plots and correlation (*R*) of A375 viability (raw luminescence values) in the primary resistance screens. Colors distinguish viral screening plates. **d**, Heat map summary of controls and candidate resistance genes identified in primary resistance screens. Protein class and ORF class are indicated (positive control, red; negative control, yellow;

experimental ORF, black). Asterisk (*) identifies two genes whose empirical sequence is significantly divergent from its annotated reference sequence.
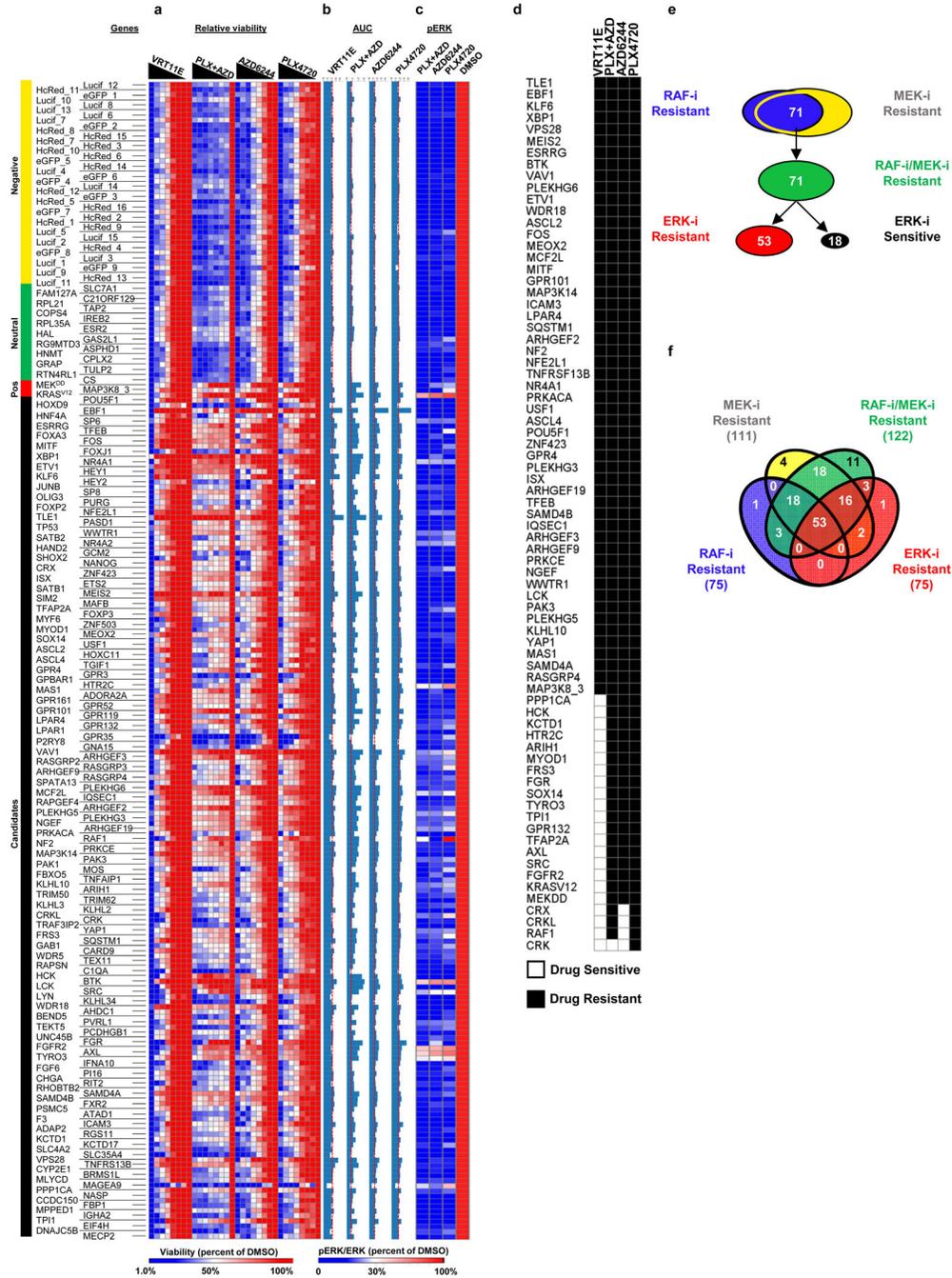
Extended Data Figure 3. Patterns of drug resistance induced by candidate resistance genes
a, Heat map displaying the percent rescue (viability in drug/viability in DMSO) for each candidate resistance ORF and control ORFs in the presence of log-fold concentrations of the indicated MAPK-pathway inhibitor. These data were used to generate drug sensitivity curves, for which **b**, the area under the curve was calculated (red dashed lines denote significance thresholds). **c**, Heat map showing ERK phosphorylation data for all candidate resistance genes and controls in A375. **d**, Matrix of genes ectopically expressed in A375 (vertical axis) versus treatment condition (horizontal axis). Sensitivity is defined as yielding

an area under the curve z-score of <1.96, resistance is defined as z >1.96 (*p*<0.05). **e**, Venn diagram showing the overlap of validated resistance genes, grouped by MAPK-pathway inhibitor, in A375. **f**, Schematic showing the number of validated genes that confer resistance or sensitivity to indicated MAPK-i.
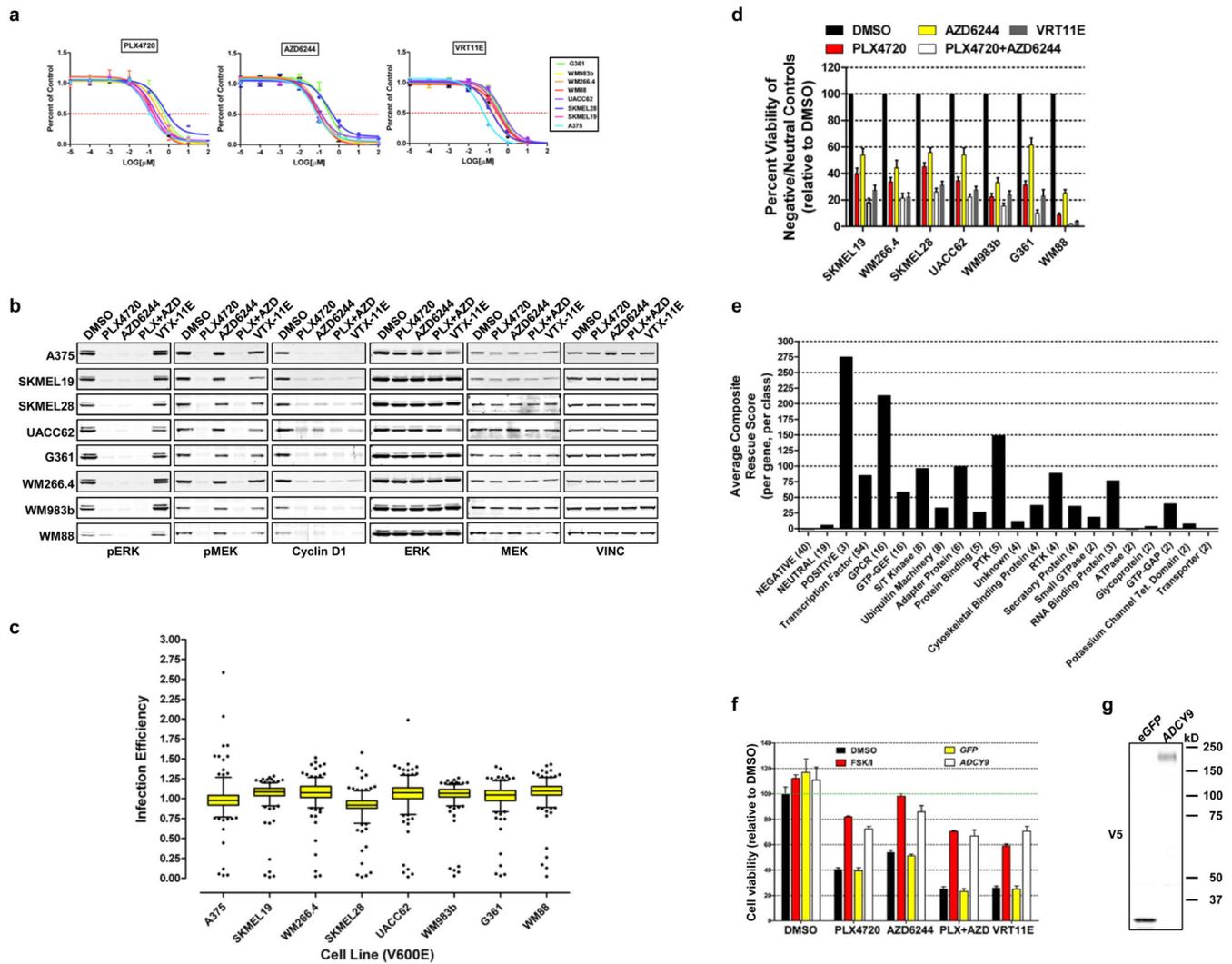
Extended Data Figure 4. Broad validation of candidate resistance genes in a panel of BRAF^{V600}-mutant melanoma cell lines

a, Drug sensitivity curves for PLX4720, AZD6244 and VRT11E in the panel of 8 BRAF^{V600E}-mutant malignant melanoma cell lines used for the primary and validation screening experiments (described in Main Fig. 2). Error bars represent s.d. of mean, n=6 technical replicates. **b**, Western blot analysis following treatment with indicated MAPK-i in the panel of 8 BRAF^{V600E}-mutant malignant melanoma cell lines used in a. **c**, Box plot of all candidate and control ORF infection efficiencies in the panel of 8 cell lines used in the validation screening experiments. Center line represents the median value, box defines the 25th–75th percentile and whiskers define the 5–95% confidence interval. Outliers are shown as individual data points. **d**, Summary of the cellular viability (relative to DMSO) of negative and neutral control genes observed in validation screens. Bar graph shows the average viability (relative to that of DMSO treatment) of each cell line when expressing the 59 negative and neutral control genes included in all validation screening experiments. Error bars represent s.d. of mean, each measured in technical duplicates. **e**, Average composite rescue score of each class of proteins identified among the resistance candidates (relates to

Main Fig. 2). Number of genes within each protein class is shown in parentheses. **f**, *ADCY9* was identified as a resistance candidate in the primary resistance screen, but was a DNA failure in our independent prep of candidate virus. Therefore, *ADCY9* was not included in the high throughput validation screens, but was included in all subsequent validation work. These data show that *ADCY9* is able to confer resistance to all tested MAPK-i to a similar degree as forskolin/IBMX treatment. Error bars represent s.d. of mean, n=6 technical replicates. **g**, Western blot analysis of the expression of V5-epitope tagged *eGFP* and *ADCY9* in WM266.4.
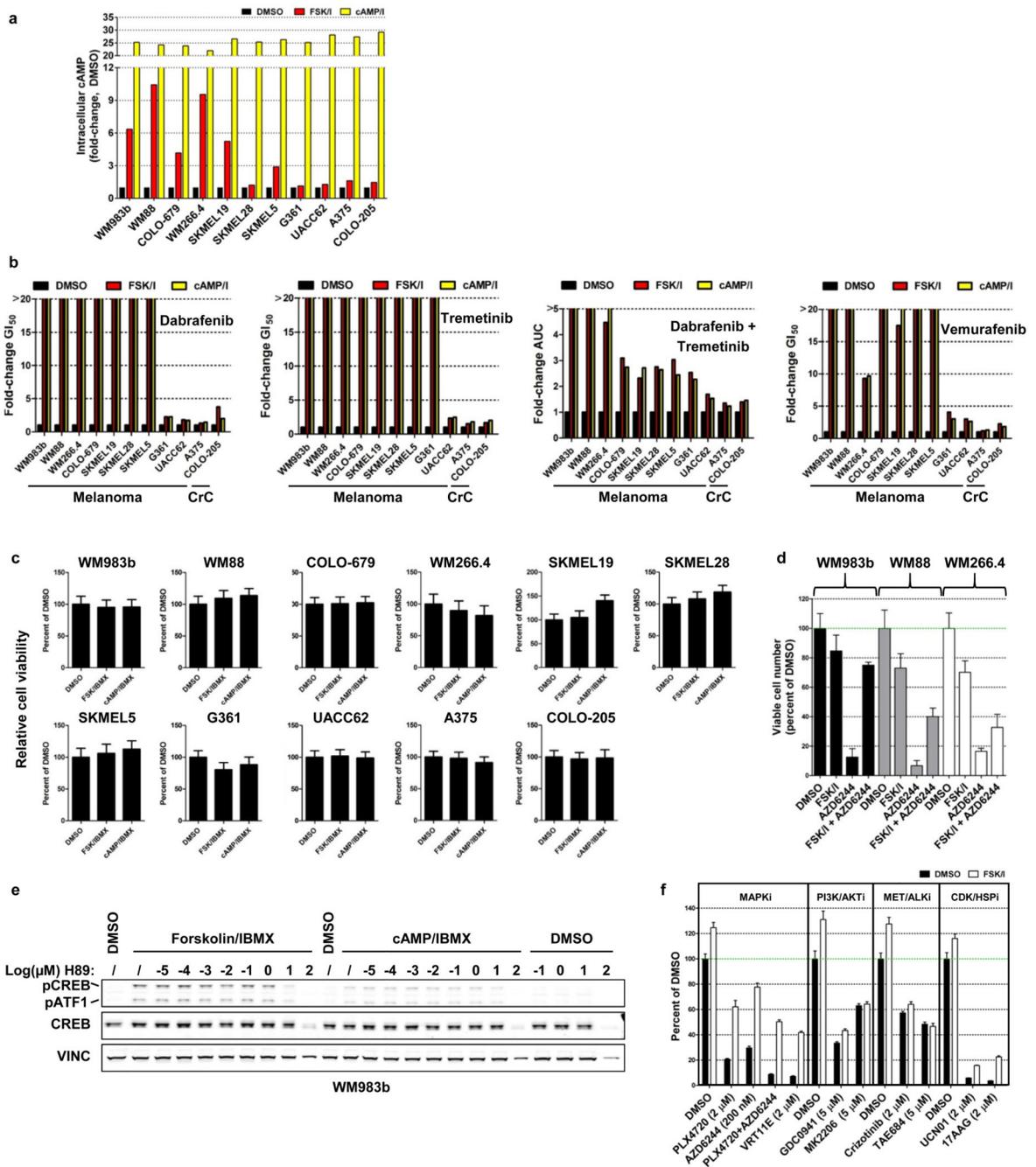
Extended Data Figure 5. Cyclic AMP induces CREB/ATF1 phosphorylation and induces MAPK-pathway inhibitor resistance

a, Mean fold-change in intracellular cAMP following treatment with forskolin + IBMX (FSK/I) or dbcAMP + IBMX (cAMP/I) using a competitive cAMP ELISA assay (n=2 technical replicates, representative of 2 independent experiments). **b**, Bar graphs showing the change in the half-maximal inhibitory concentration (GI_{50}) of $BRAF^{V600E}$-mutant cell lines treated with escalating doses of indicated MAPK-pathway inhibitor in the presence of vehicle (DMSO), forskolin/IBMX (FSK/IBMX) or dbcAMP/IBMX (cAMP/IBMX). **c**,

Relative cell viability (percent of DMSO) following FSK/IBMX or cAMP/IBMX treatment in the absence of MAPK-pathway inhibitor treatment. Error bars represent s.d. of mean, n=8 technical replicates. Data is representative of 2 independent experiments. **d**, Number of viable cells treated with the indicated compounds in the presence of vehicle (DMSO) or forskolin and IBMX (FSK/I). Error bars represent s.d. of mean, n=3 technical replicates. **e**, Immunoblot analysis of WM983b following pre-treatment with the PKA inhibitor H89 and stimulation with forskolin and IBMX. **f**, Viability of WM266.4 treated with the indicated compounds and doses in the presence of vehicle (DMSO) or forskolin and IBMX (FSK/I). Error bars represent s.d. of mean, n=6 technical replicates.
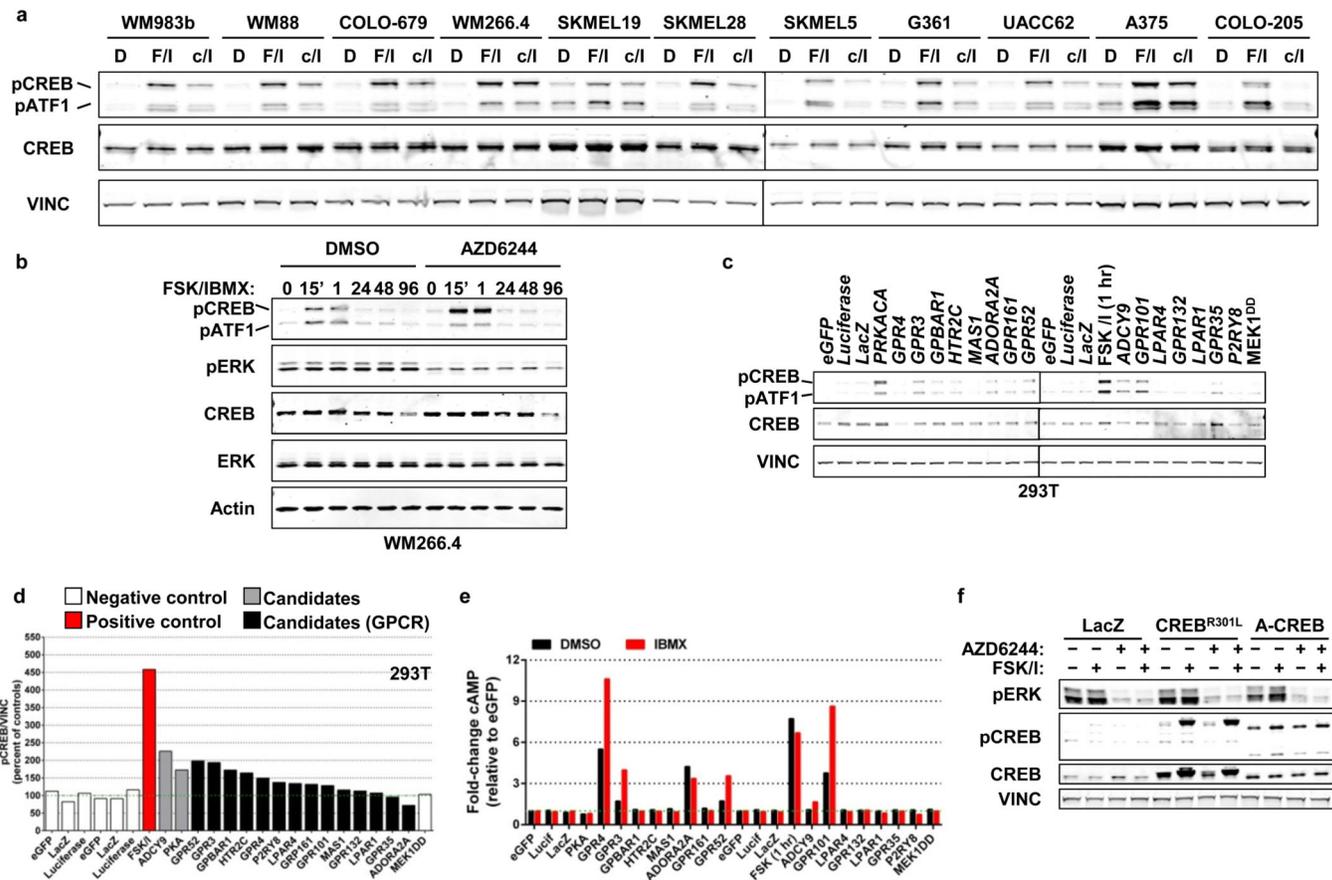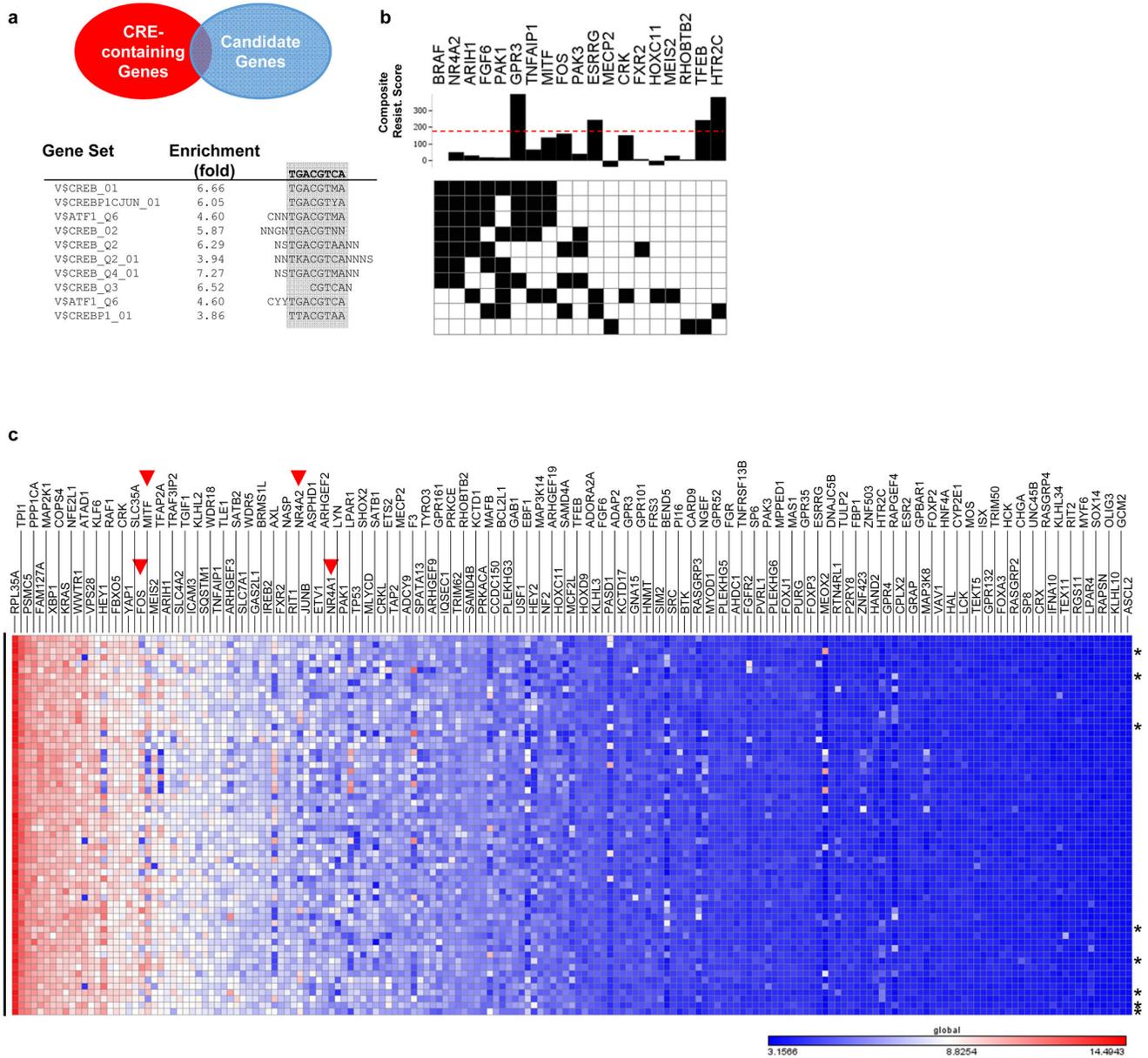
Extended Data Figure 6. Candidate GPCR/PKA pathway genes induce cAMP and CREB/ATF1 phosphorylation

a, Western blot of BRAF^{V600}-mutant melanoma cell lines stimulated with forskolin/IBMX or cAMP/IBMX. **b**, Western blot analysis of WM266.4 treated with AZD6244, followed by stimulation with forskolin and IBMX (FSK/IBMX). **c**, Western blot analysis of 293T lysates transfected with indicated genes or stimulated with forskolin/IBMX. **d**, Quantification of immunoblot analyses of 293T transiently transfected with the indicated expression constructs, pre-treated with IBMX (arbitrary units, n=2 biological replicates). **e**, Mean control or candidate gene-induced cAMP production was measured following transfection of 293T with indicated expression constructs or treatment with forskolin and IBMX (FSK/I). cAMP levels were determined using an immuno-competition assay in the presence (red bars) or absence (black bars) of IBMX (n=2 technical replicates, data is representative of three independent experiments). The green dashed line represents levels of cAMP in negative controls (eGFP, Luciferase, LacZ). **f**, Western blot analysis of WM266.4 expressing indicated constructs and treated with AZD6244 and/or forskolin/IBMX (FSK/IBMX).

a

| Patient ID#	Mutation	Site of Biopsy	Treatment	Response	Time to progression (months)
6	BRAF	Right leg dermal metastasis	dabrafenib + tremetinib	PR (-59.9%)	21, ongoing 24.5 mos
7	BRAF	Right flank subcutaneous metastasis	dabrafenib + tremetinib	CR (100%)	17, ongoing 24.5 mos
10	BRAF	Left shoulder subcutaneous metastasis	dabrafenib + tremetinib	SD (-13%)	3
12	BRAF	Right arm subcutaneous metastasis	dabrafenib + tremetinib	PR (-85.8%)	12
13	BRAF	Right chest subcutaneous metastasis	dabrafenib + tremetinib	PR (-57.9%)	9, stroke
14	BRAF	Left submandibular nodal metastasis	dabrafenib + tremetinib	PR (-64.9%)	8, lost to follow-up
16	BRAF	Right shoulder subcutaneous metastasis	dabrafenib + tremetinib	SD (-19.5%)	11
17	BRAF	Left iliac lymph nodal metastasis	vemurafenib	PR (-71.7)	15
24	BRAF	Midline chest subcutaneous metastasis	vemurafenib	PR (-53%)	2
26	BRAF	Right adrenal metastasis	dabrafenib + tremetinib	SD (-22.8%)	stopped due to hepatic toxicity after 2 mos
27	BRAF	Left neck nodal metastasis	dabrafenib + tremetinib	PR (-59.7%)	8
28	BRAF	Left back dermal metastasis	vemurafenib	No data	24
29	BRAF	Liver metastasis	dabrafenib + tremetinib	PR (-79%)	9

Extended Data Figure 7. CREB activity is regulated in the context of drug treatment in patient biopsies

a, Summary of patient sample characteristics. **b**, Immunoblot analysis of lysates extracted from BRAF^{V600E}-mutant human tumors biopsied pre-initiation of treatment (P), following 10–14 days of MAPK-inhibitor treatment (on-treatment, O) or following relapse (R). MAPK-inhibitor therapy is noted (vemurafenib, RAF inhibitor; dabrafenib, RAF inhibitor; tremetinib, MEK inhibitor). **c**, Comparison of quantified pCREB and pATF1 from b, shown as individual tumors. **d**, Statistical analysis of pATF1 and pCREB as in c, normalized to Pre-treatment levels. Samples analyzed are restricted to the subset of the biopsies that are patient matched, lesion-matched and treatment-paired *p < 0.0023, by 1-tailed T-test. **e**, Immunoblot analysis of WM266.4 following treatment with forskolin and IBMX (FSK/I) or dbcAMP and IBMX (cAMP/I) in the presence of vehicle (DMSO) or indicated MAPK-i.

Extended Data Figure 8. Identification of candidate resistance genes that are co-regulated by MAPK- and cAMP/PKA- signaling pathways

a, Candidate and neutral control genes containing cAMP response elements (CREs) were identified using gene sets extracted from MSigDB. Fold enrichment of the percent of CRE-containing genes in candidates over all genes screened for each gene set are noted. **b**, Matrix of CRE and candidate genes indicates the presence (black box) or absence (white box) of indicated CRE. Composite resistance score for each gene (summarized in Fig. 2c) is noted. Red dashed line indicates a composite resistance score of 50. **c**, Global endogenous mRNA expression (Log$_2$ RMA) of candidate and neutral control genes across a panel of melanoma cell lines. Red arrows identify the four genes hypothesized to be regulated by both the MAPK-pathway and the cAMP/PKA/CREB pathway in melanoma: MITF, FOS, NR4A1

and NR4A2. Asterisks identify the subset of cell lines used in for validation and primary screens.
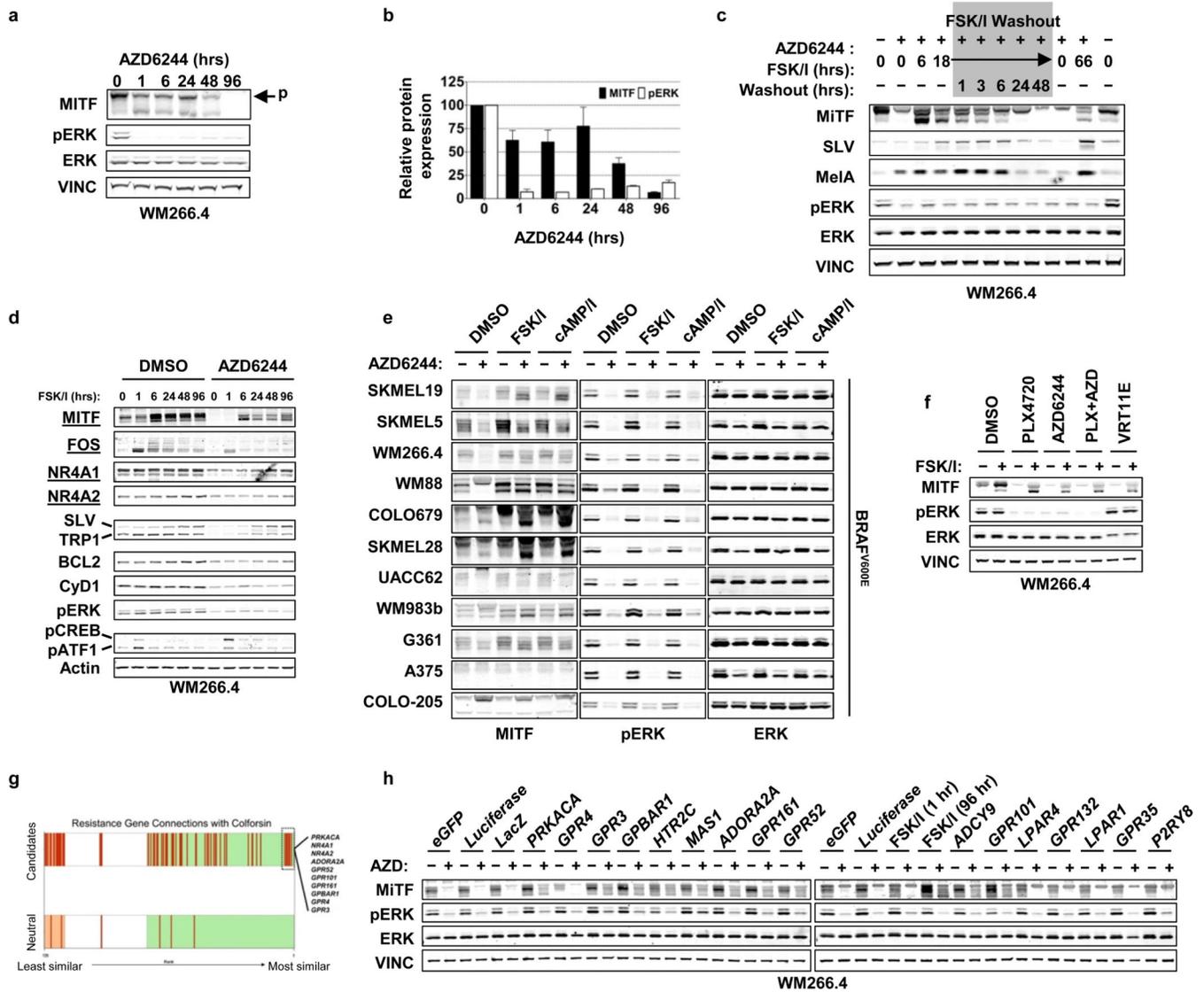
Extended Data Figure 9. cAMP/PKA regulation of MITF mediates resistance to MAPK pathway inhibition

a, Immunoblot analysis and **b**, quantification in lysates from WM266.4 cells treated as indicated. Arrow indicates the slower migrating, phosphorylated form of MITF, error bars represent s.d. of mean, n=3 biological replicates. **c**, Western blot analysis of WM266.4 following treatment with AZD6244 and stimulated for the indicated times with forskolin/IBMX. Forskolin/IBMX was washed out of the cells and replenished with normal growth media. Cell lysates were collected at the indicated times. **d**, Immunoblot analysis of WM266.4 cells following treatment with forskolin/IBMX (FSK/I) for the indicated times in the presence of vehicle (DMSO) or MEK-i. Genes identified in resistance screens are underlined. **e**, Immunoblot analysis of a panel of BRAF[V600]-mutant malignant melanoma cell lines following treatment with AZD6244 in the presence of vehicle (DMSO), forskolin/IBMX (FSK/I) or dbcAMP/IBMX (cAMP/I). **f**, Immunoblot analysis of WM266.4 cells following treatment with forskolin/IBMX (FSK/I) in the presence of vehicle (DMSO) or

indicated MAPK-pathway inhibitor. **g**, Gene signatures for all candidates and controls were generated in A375 and compared to the signatures of cAMP-stimulating small molecules, including forskolin and its water-soluble derivative, colforsin. Individual genes are grouped as Candidates or Neutral controls, with each gene represented by a vertical line. Genes are ranked by similarity with colforsin, with #1 being the most similar. A subset of the most similar genes is noted. **h**, Immunoblot analysis of WM266.4 after viral expression of the indicated genes or treatment with forskolin/IBMX (FSK/I) in the presence of vehicle (DMSO) or AZD6244.
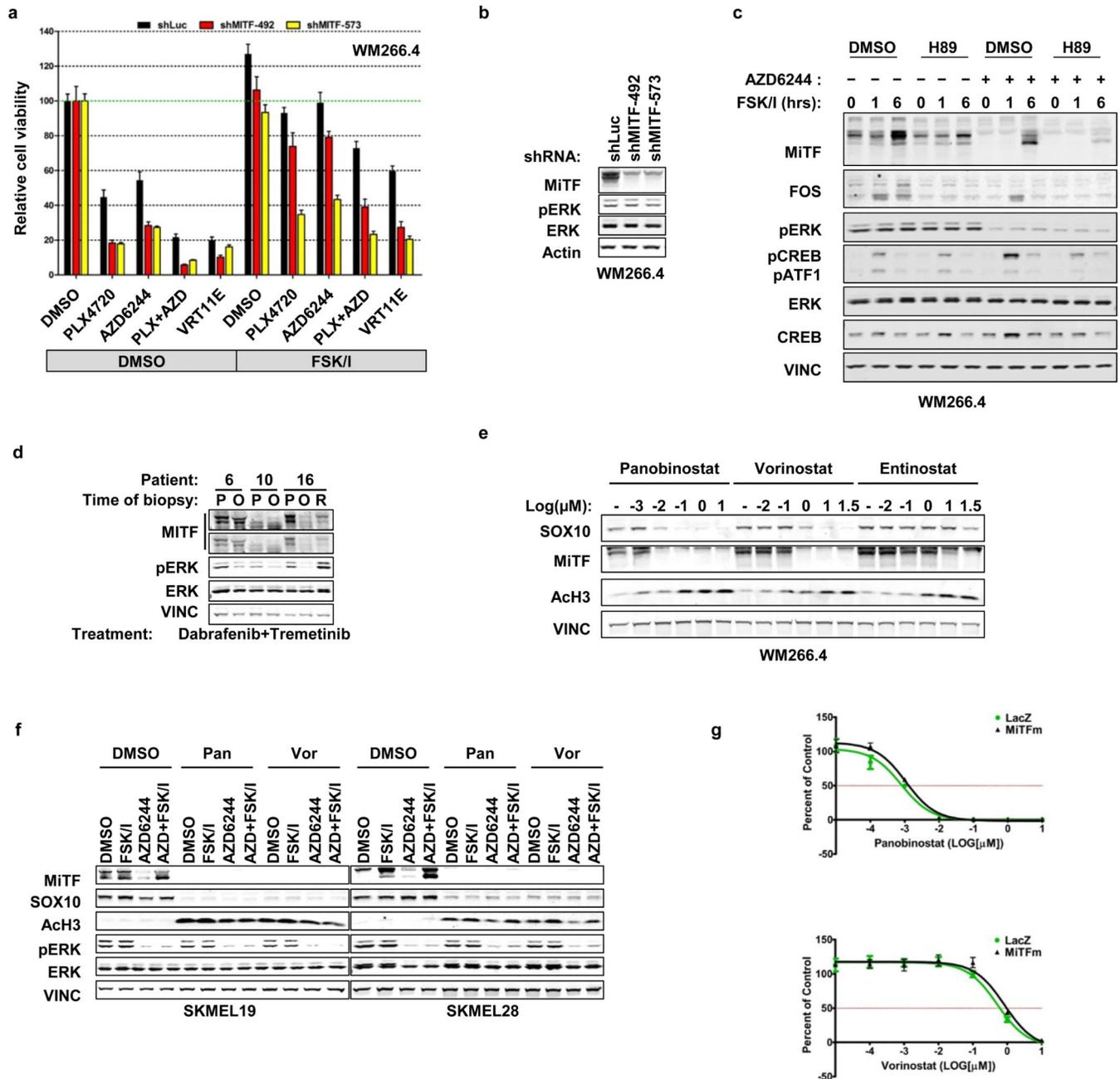
Extended Data Figure 10. Inhibition of PKA or MITF impairs cAMP-mediated resistance to MAPK pathway inhibitors

a, Cell viability of WM266.4 expressing a control shRNA (shLuciferase) or shRNAs targeting MITF treated with indicated MAPK-i and concomitant treatment with either DMSO or forskolin/IBMX (FSK/I). Error bars represent s.d. of mean, n=6 technical replicates, data is representative of two independent experiments. **b**, Western blot analysis of WM266.4 expressing the shRNA-constructs used in a. **c**, Western blot analysis of WM266.4 treated with AZD6244, followed by pre-treatment with DMSO or H89 and subsequent stimulation with forskolin/IBMX (FSK/I) for the indicated times. **d**, Immunoblot analysis of lysates extracted from human BRAF[V600E] positive melanoma biopsies. Biopsies were

obtained prior to treatment (P), on MAPK-inhibitor treatment for 10–14 days (on-treatment, O) or following relapse (R). **e**, Immunoblot analysis of WM266.4 treated with the indicated concentration of HDAC-inhibitor. **f**, Immunoblot analysis of SKMEL19 and SKMEL28 in the presence of vehicle (DMSO) or AZD6244, followed by treatment with the indicated HDAC-inhibitor (panobinostat; Pan, vorinostat; Vor) and subsequent stimulation with forskolin/IBMX (FSK/I). **g**, Drug sensitivity curves of Panobinostat and Vorinostat in WM266.4 expressing LacZ or MITFm. Error bars represent s.d. of mean, n=3 technical replicates.